

# Role of the fast Ar atoms, Ar<sup>+</sup> ions, and metastable Ar atoms in a hollow cathode glow discharge: Study by a hybrid model

N. Baguer,<sup>a)</sup> A. Bogaerts, and R. Gijbels

*Department of Chemistry, University of Antwerp (UIA), Universiteitsplein 1, B-2610 Wilrijk-Antwerp, Belgium*

(Received 25 March 2003; accepted 2 June 2003)

The role of the fast Ar atoms, Ar<sup>+</sup> ions, and metastable Ar atoms in a cylindrical hollow cathode discharge (HCD) is studied based on a self-consistent model. The model comprises submodels based on the principle of Monte Carlo and fluid simulations. With Monte Carlo models the movement of the fast electrons, fast Ar atoms, and fast Ar<sup>+</sup> ions as particles is described, while with the fluid models, the slow electrons, ions, and metastable atoms are treated as a continuum. Typical results are, among others, the fast atom, fast ion, and fast electron excitation and ionization rates, the electron, ion, and metastable atom densities and fluxes, the energy distribution function of the fast atoms, fast ions, and fast electrons, and the electric field and potential distribution. Also the relative importance of different processes determining the metastable density in an Ar HCD is analyzed, as well as the influence of the fast atoms and fast ions on the discharge properties. © 2003 American Institute of Physics. [DOI: 10.1063/1.1594276]

## I. INTRODUCTION

Hollow cathode discharges (HCD) are extensively used in laser technologies,<sup>1,2</sup> spectroscopic analysis,<sup>3,4</sup> and plasma processing (ion etching, thin film deposition, surface treatment).<sup>5,6</sup> Many of these applications are based on the sputtering of the cathode material by high-energy ions and atoms. In HCDs, the loss of energetic particles [to the anode(s) and to the walls] is considerably reduced due to its geometric configuration.<sup>7,8</sup> Hence most of the energy of the fast particles is spent inside the discharge, i.e., for the production of new electron-ion pairs, excitation collisions, charge transfer collisions, etc. This makes the HCD a very efficient and useful discharge to obtain high rates of sputtering. In this article we will focus on the study of the ions and fast atoms, due to the importance of these species for the sputtering of the cathode material. Moreover, we will also describe the behavior of the metastable atoms.

A very important step in the study of the role of ions and atoms in glow discharges (GD) was achieved by the experimental and theoretical work of Davis and Vanderslice,<sup>9</sup> who pointed out the relevance of symmetric charge transfer collisions in determining the ion and atom energy distribution in the cathode dark space (CDS). Since then, different theoretical and computational approaches have been developed in order to study more precisely other processes, which are responsible for determining the energy distribution, fluxes, densities, etc. of these species in GDs. For example, a theoretical approach was followed in Ref. 10, where analytical formulas for the energy distribution function of ions and neutrals in the CDS were derived based on the model of Davis and Vanderslice. In Ref. 11, this model was extended, using the transport formalism, to account for electron impact ionization collisions in the CDS. In Ref. 12 a transport model

combined with a phenomenological method (viscous drag fluid model) was used to describe rf discharges. In transport models it is assumed that the particle energy is in hydrodynamic equilibrium with the local field.<sup>13</sup> However, when using such a model in the CDS, the electron energy distribution of the fast electrons, which are responsible for most of the ionization collisions, is not correctly calculated, and consequently the calculated electron collision rates are not very reliable. With Monte Carlo models (MC)<sup>14,15</sup> the microscopic nature of a collision can be considered. The particles are followed one after another and the collision rates are calculated based on the energy-dependent cross sections. Hence a correct energy distribution function for the energetic particles can be calculated. However, a MC model is not self-consistent because the electric field is not calculated in the model, but needs to be given as input. In Ref. 16 a MC model was used to calculate energy and angular distributions of He and Ar ions in the CDS considering symmetric charge transfer and elastic collisions. With the particle-in-cell-Monte Carlo (PIC-MC) method,<sup>17</sup> the problem can be solved self-consistently. The collision rates are calculated based on the energy-dependent cross section, and the particle energy is calculated from the electric field, which is obtained self-consistently from Poisson's equation using the charged species densities. This method is very time-consuming because a large number of particles should be followed for statistically valid results. Another way of solving the problem self-consistently is the so-called hybrid model,<sup>18,19</sup> e.g., a MC model combined with a fluid model (i.e., a transport model, where the Poisson equation is solved together with the continuity and flux equations for ions and electrons).<sup>20,21</sup> Such a hybrid model combines the advantages of both methods and it is considerably faster than a PIC-MC model.<sup>22</sup> Hybrid models for describing the role of fast ions, neutrals, and electrons were applied to GDs with planar cathode in hydrogen<sup>23</sup> and argon,<sup>24,25</sup> respectively. In the present article we will

<sup>a)</sup>Electronic mail: baguer@uia.ua.ac.be

apply a similar approach as in Ref. 24 to a cylindrical HCD in Ar to obtain the energy distribution of ions and fast atoms arriving at the cathode walls. These distributions will be used in a future work to calculate the density of the sputtered species, i.e., the sputtered atoms and ions from the cathode material.

## II. DESCRIPTION OF THE MODELS

### A. Assumptions of the model

The discharge gas was assumed to be argon at room temperature and uniformly distributed throughout the discharge, i.e., the thermal motion of the gas atoms is neglected. The other species considered in the model are singly charged positive ions ( $\text{Ar}^+$ ), metastable Ar atoms, fast and slow electrons, and fast Ar atoms ( $\text{Ar}_f$ ). The  $\text{Ar}_f$  atoms are formed by elastic collisions of  $\text{Ar}^+$  ions with the background gas and are assumed to have energies higher than 1 eV. The electrons are split up in two groups:<sup>18</sup> the fast electrons, with high enough energy to cause inelastic collisions, and the slow electrons, which do not have enough energy. The energy threshold for considering electrons as fast particles was 1.8 eV, which corresponds to the excitation energy from the metastable levels. The fact that we consider a fraction of the Ar atoms as fast particles does not contradict the assumption that the gas is uniformly distributed throughout the discharge, because the fast Ar atom density is much lower than the density of the discharge gas.<sup>25</sup> The two metastable levels of Ar,  $^3P_2$ , and  $^3P_0$ , which are lying at 11.55 and 11.72 eV above the ground state, respectively, have been combined into one collective level, lying at 11.55 eV.<sup>26</sup> This assumption was made based on the fact that the  $^3P_0$  level was considerably less populated than the  $^3P_2$  level<sup>27</sup> and for our purpose only the total metastable density is important.

The hybrid model presented here is a combination of two methods: MC and fluid. The MC method is used to describe the motion of the fast particles, i.e., the ions in the CDS, and the fast electrons and fast atoms in the entire discharge. The fluid model treats the ions and metastable Ar atoms in the entire discharge, while the slow electrons are only treated in the negative glow (NG). Note that the slow electrons are only present in the NG, because in the CDS they gain additional energy from the electric field so that they become fast again. Due to the low degree of ionization of the discharge gas<sup>15,24,28</sup> the collision processes incorporated in the MC models are concerned only with the interaction of the fast species with the background gas, i.e., the movement of the ions and electrons can be considered independent from each other and treated separately in corresponding MC codes.<sup>23</sup> The collision processes considered in this work are for the fast electrons: elastic collisions, excitation, and ionization from the ground and metastable state. For the ions: elastic collisions (including symmetric charge transfer), excitation to the metastable state, and ionization from the ground state are taken into account. Finally, for the fast atoms: elastic collisions, excitation to the metastable state, and ionization from the ground state are considered.

### B. Monte Carlo model for the fast electrons

This model is, in general, the same as described in Ref. 28, but the following modifications have been made.

- (1) Electron impact excitation and ionization from the Ar metastable levels have been added as collision processes.
- (2) Electron impact excitation from the ground state to the metastable levels was explicitly considered. All cross sections of these collisions were taken from Refs. 29–31.
- (3) Besides the new cascade electrons created by electron impact ionization also the electrons created by atom and ion impact ionization and metastable–metastable ionization collisions (see below) were followed.
- (4) The position at which the secondary electrons are ejected from the cathode walls was determined based on the distribution of the metastable and ion fluxes to the walls.

### C. Monte Carlo model for the fast ions

The MC simulation of the ions is done in a similar fashion as for the electrons, but the ions are followed only as fast particles inside the CDS. The ions start at the CDS-NG boundary, or within the CDS, with an assumed initial energy of 0.05 eV and a velocity direction parallel to the electric field.<sup>15</sup> For the ions starting at the CDS-NG interface the initial position is determined from the radial and axial ion flux diffusing from the NG to the CDS, as calculated in the charged particle fluid model (see below). As a result of the electron impact ionization and metastable–metastable ionization collisions, also some ions are created inside the CDS. The initial position of these ions is obtained from the corresponding ionization rates (calculated in the fast electron MC model and in the fluid model for metastable atoms, respectively). Also the new ions created as a result of ion or fast atom impact ionization are followed.

During each time-step the trajectory of the ions is calculated with Newton's laws:

$$\mathbf{r} = \mathbf{r}_0 + \mathbf{v}_0 \Delta t + \frac{q\mathbf{E}}{2m} \Delta t^2, \quad \mathbf{v} = \mathbf{v}_0 + \frac{q\mathbf{E}}{m} \Delta t, \quad (1)$$

where  $\mathbf{E}$  is the electric field,  $m$  is the Ar atomic mass,  $q$  is the particle charge,  $\Delta t$  is the time interval, and  $\mathbf{r}_0$ ,  $\mathbf{v}_0$  and  $\mathbf{r}$ ,  $\mathbf{v}$  are the position and velocity vectors before and after  $\Delta t$ , respectively.

The probability of collision during the time step  $\Delta t$  is calculated by:  $P = 1 - \exp[-\Delta s n_{\text{Ar}} \sigma_t(\varepsilon)]$ , where  $\Delta s$  is the distance traveled by the ion with energy  $\varepsilon$  during the interval  $\Delta t$ ,  $n_{\text{Ar}}$  is the density of the Ar atoms in the ground state, and  $\sigma_t(\varepsilon)$  is the total  $\text{Ar}^+$  scattering cross section. The cross sections for elastic collisions (including symmetric charge transfer) are taken from Ref. 32, whereas the cross sections for ion impact ionization and for excitation to the metastable levels were adapted from Ref. 33. The calculated collision probability is compared with a random number ( $rn$ ), uniformly distributed in the interval between 0 and 1. If  $rn < P$ , a collision occurs. To determine the kind of collision a second  $rn$  is generated and compared with the relative probability of each collision. Due to the lack of information about

differential angular scattering cross sections, we have assumed the elastic scattering as isotropic in the center of mass<sup>32</sup> and we have neglected the angular scattering in inelastic collisions. The latter assumption (i.e., conservation of velocity direction after ion impact ionization and excitation) will have almost no influence on the mean energy of the ions and atoms. Indeed, the energy is primarily determined by the elastic (including charge transfer) collisions, due to their higher cross section at the energy range of interest here.<sup>9,34</sup> After each collision, the new ion energy and velocity direction are calculated depending on the type of collision.

(a) Elastic collision: In this model the elastic differential scattering cross section in the center of mass is approximated<sup>32</sup> by the sum of two components: (i) a backward (or 180°) scattering component and (ii) an isotropic component.

(i) The backward scattering component of elastic scattering and a cold (or stationary) atom results in a slow ion and a fast atom. The new ion starts at rest and the initial velocity direction is assumed to be parallel to the electric field. The new created fast atom is assumed to have the energy and velocity direction equal to the original ion<sup>9</sup> and it will be followed in the MC model for fast atoms (see below). At high collision energies, this backward scattered component is equal to the charge transfer cross section. At low energies this component becomes very small as the elastic scattering becomes more isotropic.

(ii) Based on the assumption of isotropic scattering in the center-of-mass frame, the polar  $\chi$  and azimuthal  $\phi$  angles of scattering with respect to the incident ion velocity direction are calculated as follows:  $\chi = 0.5 \arccos(1 - 2rn)$ ,  $\phi = 2\pi rn$ . From these angles the new velocity angles are found by transformation of the coordinate frame of reference. The ion energy is  $E = E_{\text{ini}}[1 - (\sin \chi)^2]$ , where  $E_{\text{ini}}$  is the incident ion energy. If the transferred energy to the background atom is higher than the threshold energy, i.e.,  $E_{\text{ini}}(\sin \chi)^2 > 1 \text{ eV}$ , the atom is considered as a fast particle and hence followed in the MC code for fast atoms (see below).

(b) Excitation collision: No change in velocity direction is assumed and the energy after the collision is calculated as:  $E = E_{\text{ini}} - E_{\text{exc}}$ .

(c) Ionization collision: It is assumed that the energy is shared equally between the projectile and the new formed ion, so that  $E = (E_{\text{ini}} - E_{\text{ion}})/2$ . Further, like for the excitation collision, no change in velocity direction is assumed. The newly created ion is followed also in this MC model.

This procedure of following the ions with Newton's laws and describing their collisions with cross sections and  $rn$  is repeated until the ions collide at the cathode walls or at the anode, where they are neutralized and disappear from the calculations.

## D. Monte Carlo model for the fast atoms

This subprogram handles the atoms formed from elastic (including charge transfer) collisions from the  $\text{Ar}^+$  ions, and which have energies above 1 eV. Atoms with energy below 1 eV are assumed to belong to the thermalized group. The neutral atoms are not directed to the cathode walls because they do not feel the electric field, and hence they are followed in the entire discharge. Their trajectory is calculated also by the set of equations (1) (see above), but the term including the electric field disappears. For determining the occurrence and kind of collisions and also the energy and velocity direction after collisions, the same assumptions as for the ions were made. The collision processes considered here are elastic collision, atom impact ionization, as well as excitation from the ground state to the metastable levels. The corresponding cross sections for elastic and ionization collisions were taken from Refs. 32 and 33, respectively. For the atom impact excitation, we have not found any set of cross sections and we have assumed it to be equal to the ion impact excitation cross section to the metastable state.<sup>25</sup> The positions of the new-formed particles (ions and electrons as a result of atom impact ionization and fast atoms as a result of atom elastic collisions) are stored in an array and later treated in the corresponding codes. The fast atoms are followed until they reach the cathode or anode walls, where they can be implanted or reflected or until their energy drops below 1 eV.

## E. Fluid model for the metastable atoms

The behavior of the metastable atoms is described by a continuity and a transport equation, in which the flux is only determined by diffusion.<sup>26,35,36</sup> The different production and loss processes considered in the model are summarized in Table I.

Taking into account the production and loss processes summarized in Table I the Ar metastable atoms are described with the following balance equation:

$$\frac{\partial n_{\text{Ar}^m}}{\partial t} - D_{\text{Ar}^m} \nabla^2 n_{\text{Ar}^m} = S_{\text{prod}} - S_{\text{loss}}, \quad \text{continuity equation,} \quad (2)$$

where

$$S_{\text{prod}} = S_{e,\text{exc}} + S_{\text{Ar}^+,\text{exc}} + S_{\text{Ar}^f,\text{exc}} + k_{\text{rec}} n_e n_{\text{Ar}^+},$$

$$S_{\text{loss}} = S_{e,\text{ion},m} + S_{e,\text{exc},m} + k_{\text{que}} n_{\text{Ar}^m} n_e + 2k_{\text{met}} [n_{\text{Ar}^m}]^2$$

$$+ k_{2\text{B}} n_{\text{Ar}^m} n_{\text{Ar}} + k_{3\text{B}} n_{\text{Ar}^m} [n_{\text{Ar}}]^2.$$

Equation (2) is discretized and solved with the Thomas algorithm<sup>42</sup> assuming as boundary condition  $n_{\text{Ar}^m} = 0$  (the same at anodes and cathode).

## F. Fluid model for the ions and slow electrons

The description of this model is already given in Ref. 28. Here we should only point out that because other ionization collisions were added (see above), the production of charged particles was enhanced and consequently, the source terms of the continuity equations include all of these processes.

TABLE I. Production and loss processes considered in the fluid model for metastable Ar atoms.

Production processes		Rates or rates coefficients
$\text{Ar} + e_f \rightarrow \text{Ar}^m + e_f$	electron-impact excitation	$S_{e,\text{exc}}$ [calculated in MC- $e$ ]
$\text{Ar} + \text{Ar}^+ \rightarrow \text{Ar}^m + \text{Ar}^+$	ion-impact excitation	$S_{\text{Ar}^+,\text{exc}}$ [calculated in MC- $\text{Ar}^+$ ]
$\text{Ar} + \text{Ar}^f \rightarrow \text{Ar}^m + \text{Ar}^f$	atom-impact excitation	$S_{\text{Ar}^f,\text{exc}}$ [Calculated in MC- $\text{Ar}^f$ ]
$\text{Ar}^+ + e \rightarrow \text{Ar}^m + h\nu$	radiative recombination	$k_{\text{rec}} = 1 \times 10^{-11} \text{ cm}^3 \text{ s}^{-1\text{a}}$
Loss processes		
$\text{Ar}^m + e_f \rightarrow \text{Ar}^+ + 2e_f$	electron-impact ionization	$S_{e,\text{ion},m}$ [calculated in MC- $e$ ]
$\text{Ar}^m + e_f \rightarrow \text{Ar}^* + e$	electron impact excitation to higher energy levels	$S_{e,\text{exc},m}$ [calculated in MC- $e$ ]
$\text{Ar}^m + \text{Ar}^m \rightarrow \text{Ar}^+ + \text{Ar} + e_f$	metastable–metastable collision	$k_{\text{met}} = 6.4 \times 10^{-10} \text{ cm}^3 \text{ s}^{-1\text{b}}$
$\text{Ar}^m + e \rightarrow \text{Ar}^* + e$	electron quenching	$k_{\text{que}} = 2 \times 10^{-7} \text{ cm}^3 \text{ s}^{-1\text{c}}$
$\text{Ar}^m + \text{Ar} \rightarrow \text{Ar} + \text{Ar}$	two-body collision	$k_{2\text{B}} = 2.3 \times 10^{-15} \text{ cm}^3 \text{ s}^{-1\text{d}}$
$\text{Ar}^m + 2\text{Ar} \rightarrow \text{Ar}_2^* + \text{Ar}$	three-body collision	$k_{3\text{B}} = 1.4 \times 10^{-34} \text{ cm}^6 \text{ s}^{-1\text{d}}$
Diffusion to the walls, followed by deexcitation at the walls		$D_{\text{Ar}^m} = 54 \text{ cm}^2 \text{ s}^{-1\text{e}}$

<sup>a</sup>Taken from Ref. 38.<sup>b</sup>Taken from Ref. 37.<sup>c</sup>Taken from Ref. 39.<sup>d</sup>Taken from Ref. 40.<sup>e</sup>Taken from Ref. 41.

### G. Coupling of the submodels

First the MC model for the  $\text{Ar}^+$  ions and fast Ar atoms (MC- $\text{Ar}^+ - \text{Ar}_f$ ) is run. As input this subprogram requires the number of ions created inside the CDS, and the ions starting at the CDS-NG interface, as well as the electric field distribution in the CDS. They were taken from a previous run, for the same conditions, where only fast electron impact ionization was considered.<sup>28</sup> This model yields, among others: the fast ion and fast atom impact ionization rates (giving the position for the newly created electron to be followed in the MC model for fast electrons, MC- $e$ ), the ion and fast atom impact excitation rates to the metastable levels (used as input in the metastable fluid model, giving the creation rate of metastables), and the ions and fast atom energy distributions.

Second, the fluid model for the metastable atoms is run. The output of this model includes the density of the metastable level and the flux of metastable atoms bombarding the cathode ( $J^{\text{Ar}^m}$ ). These results are both used in the MC- $e$  model, i.e., to determine the electron impact ionization and excitation rates from the metastable level, and the secondary electron emission at the cathode due to the flux of metastable atoms, respectively. Moreover, the metastable fluid model yields the ionization rate due to metastable–metastable collisions, which is used in the MC- $\text{Ar}^+ - \text{Ar}_f$  model and in the MC- $e$  model to determine the starting position of the new ions and electrons, respectively.

Third, the MC- $e$  model is calculated. All the new electrons created by fast ion, fast atom, and metastable ionization collisions are followed. For the first iteration, the electric field and the ion flux to the cathode walls ( $J^{\text{Ar}^+}$ ) were taken from previous calculations for the same conditions.<sup>28</sup> The secondary electron emission coefficient ( $\gamma$ ) is calculated in the same way as described in Ref. 28. However, because the contribution of the ions, fast atoms, and metastable atoms to the formation of ion–electron pairs is explicitly calculated in this work,  $\gamma$  represents here the total ion induced secondary electron emission coefficient. Assuming that ion and meta-

stable induced secondary electron emission coefficients are similar<sup>43</sup> the electron flux at the cathode ( $J^e$ ) is calculated as  $J^e = \gamma(J^{\text{Ar}^+} + J^{\text{Ar}^m})$ . Output of the MC- $e$  model used as input in the MC- $\text{Ar}^+ - \text{Ar}_f$  model is the electron ionization rate, which gives the number of ions created by electron impact ionization. Output of the MC- $e$  model used for the metastable model are the production rate of the metastable atoms due to electron impact excitation from the ground as well as the loss rates due to electron impact excitation and ionization from the metastable level. Output of the MC- $e$  model used as input in the fluid model includes the  $\gamma$  coefficient, used to calculate the electron component of the total current at the cathode and the ion and slow electron creation rates.

Next the fluid model is run with the above source terms. It yields the ion and electron densities, the axial and radial ion and electron fluxes, and the axial and radial electric field distribution. The electric field and the ion flux to the cathode walls and to the CDS–NG interface will be used as input for the MC models. The ion and electron densities are used in the metastable model to calculate certain production and loss rates, which are not provided from the MC models.

The above four models are run iteratively, until convergence is reached. The latter is determined by the difference in the total current to the anode in two successive iterations, which should be below 1%. Typically, 3 to 4 iterations were carried out before convergence was reached.

### III. RESULTS AND DISCUSSION

The models were applied to a HCD, consisting of a cylindrical cathode closed at one end and a disk anode at the other end, separated by 0.2 cm (see Fig. 1 of Ref. 28). The discharge conditions assumed in the model were taken from experiment, i.e., the gas pressure was varied from 0.3 to 1.0 Torr, the discharge current ranged from 1 to 10 mA, and a discharge voltage between 240 and 300 V was applied to the cathode whereas the anode was grounded. The gas temperature was assumed to be 300 K.

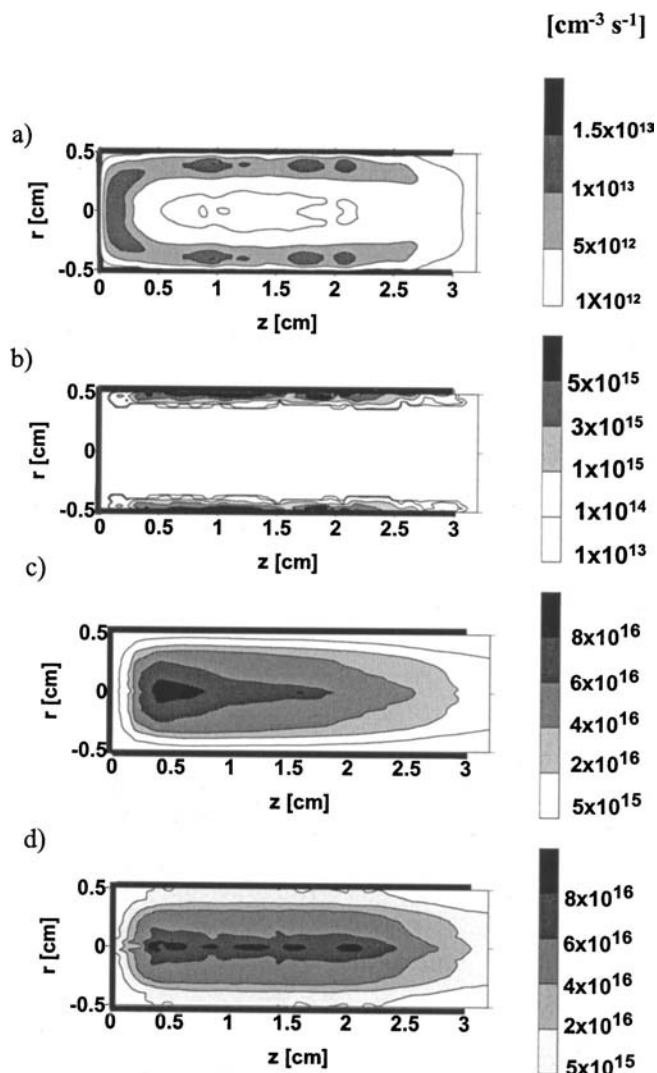


FIG. 1. Calculated two-dimensional ionization rate profiles throughout the discharge at a pressure of 0.3 Torr and a current of 9.2 mA, as a result of metastable–metastable atom collisions (a); ion and fast atom impact ionization (b); electron impact ionization, calculated when only electron collisions were considered (Ref. 28) (c); and the total ionization rate considering electron, ion, fast atom, and metastable–metastable ionization collisions (d). The hollow cathode is represented by the thick black lines from  $z=0$  cm  $z=3$  cm, whereas the anode ring is located at  $z=3.2$  cm.

To study the contribution of the various processes to the total ionization rate, Fig. 1 presents the calculated ionization rate profiles at 0.3 Torr and 9.2 mA. This condition is a representative example for all the discharge conditions investigated here. Note that the thick black lines in this figure and in all following contour plots represent the cathode walls.

The maximum in the ionization rate due to the metastable–metastable collisions [Fig. 1(a)] is observed in the center of the CDS and it is three orders of magnitude less than the maximum rate due to atom and ion impact ionization collisions [Fig. 1(b)], which take place only very close to the cathode walls. Integrated over the total discharge volume, metastable–metastable ionization represents only 0.04% of the total ionization, followed by 0.16% due to ion impact ionization and 2.8% due to fast atom impact ionization at the conditions under study here. Hence electron im-

pair ionization has a dominant contribution to the total ionization.

In previous work, it was already demonstrated that the ionization collisions inside the CDS were important, even at high currents.<sup>28</sup> In this work, where some more ionization sources are included, the importance of ionization in the CDS is even more pronounced because these additional processes are most important inside the CDS. In spite of the fact that integrated over the total discharge volume these processes contribute only for 3% to the total ionization, their influence in the discharge is larger than that, as will be shown below. Indeed, most ion–electron pairs are created, due to these processes, inside the CDS; hence these additional ions and electrons can gain energy from the electric field and contribute also to the enhancement of the total ionization. This enhancement can be observed if we compare Figs. 1(c) and 1(d). Figure 1(c) shows the total ionization rate profile when only electron impact ionization was considered, whereas Fig. 1(d) presents the total ionization rate, when also the ionization by heavy particles was included. In Fig. 1(c) the total ionization rate was less than  $5 \times 10^{15} \text{ cm}^{-3} \text{ s}^{-1}$  close to the cathode walls, whereas in Fig. 1(d) it was higher than this value close to the cathode walls (see the contour line corresponding to this value). Moreover, in Fig. 1(d) the rate profile is a bit higher in magnitude and more uniform throughout the entire length of the HCD than in Fig. 1(c). A direct measure of this enhancement in ionization rate can also be obtained from the electron multiplication coefficient, i.e., the number of electrons created in the discharge per electron ejected from the cathode due to ion and metastable induced secondary electron emission. We calculated a rise in electron multiplication coefficient, from 28, when only electron impact ionization was considered, to 42 when all other ionization processes were included as well. This represents an increase of 33% for the discharge conditions of Fig. 1.

Electron impact ionization of Ar atoms was found to be the dominant process of electron production for all the conditions investigated here. The relative contribution of the additional ionization processes to the total ionization in the discharge increases with decreasing pressure, as can be seen from Fig. 2(a). For example, at a discharge current of 9 mA and at 1 Torr pressure, it represents 0.6% of the total ionization rate, increasing to 3% at 0.3 Torr. With decreasing pressure at constant current, the CDS length increases; hence the ionization inside the CDS increases. Moreover, the discharge voltage increases also. The higher discharge voltage results in higher  $\text{Ar}^+$  ion and  $\text{Ar}_f$  atom energies and consequently in more efficient ion and atom impact ionization because the ionization cross sections increase with rising energy, in the energy range of interest here.<sup>33</sup> At constant pressure, the contribution of these processes gains in importance at currents for which the ionization inside the CDS is predominant<sup>28,44</sup> (i.e., low currents, corresponding to the step gradient of the voltage-current dependency) and also at high currents. (A higher discharge current at constant pressure arises from higher voltage.)

The influence of these new sources of ionization on the current–voltage characteristic of the discharge is small. The

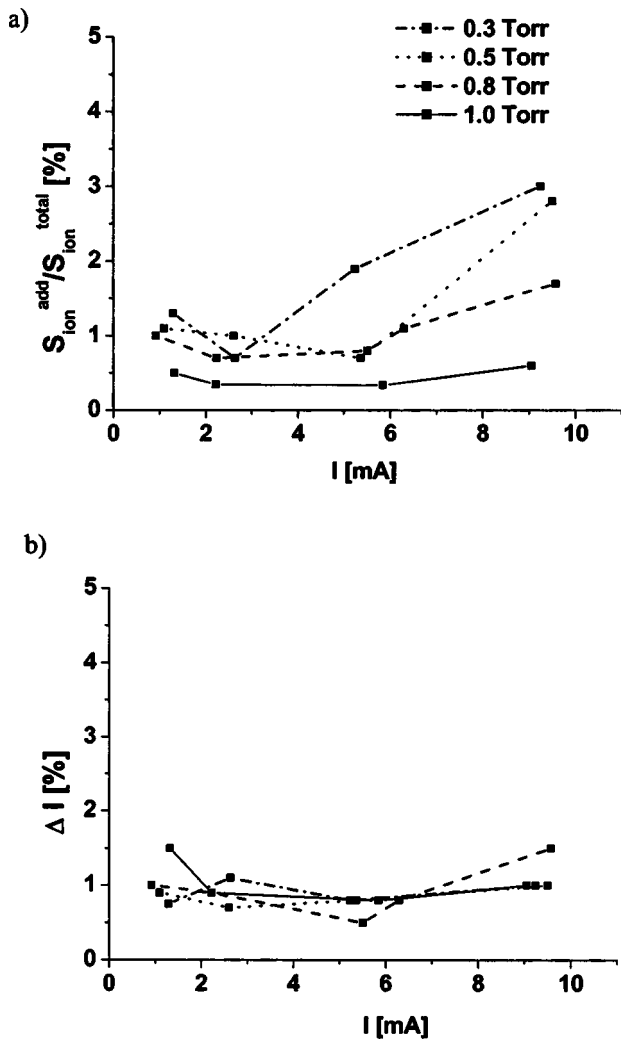


FIG. 2. (a) Calculated relative contribution (in percent) to the total ionization rate due to the ionization collisions of  $Ar^+$  ions, fast Ar atoms, and metastable Ar atoms (i.e., the additional ionization rates;  $S_{ion}^{add}$ ) for all the discharge conditions investigated here. (b) Calculated rise of the total discharge current (in percent) due to the additional ionization processes.

total rise in discharge current due to the contribution of fast atom, ion, and metastable ionization collisions is less than 2% for all the conditions investigated here, as can be seen from Fig. 2(b). Indeed, the discharge current is an integrated value, i.e., it reflects the total amount of ionization, and the added ionization processes represent only a small fraction of the total ionization in the discharge [Fig. 2(a)]. However, the additional ionization processes will have more effect on the calculation of parameters which directly depend on the ionization distribution in the CDS; i.e., the net charge density distribution in the CDS and consequently the voltage drop in the CDS, as well as the electric field and the plasma potential. Indeed, close to the cathode walls, these ionization processes determine the total ionization rate profile (see Fig. 1).

Figure 3 illustrates the radial profiles (at  $z = 1.6$  cm) of the net charge density, i.e., the  $Ar^+$  ion density minus the electron density [Fig. 3(a)], the ion and electron densities [Fig. 3(b)], the electric potential [Fig. 3(c)], and the electric field [Fig. 3(d)] at a pressure of 0.3 Torr and a current varying from 1.3 to 9.2 mA. Note that  $r = 0$  corresponds to the

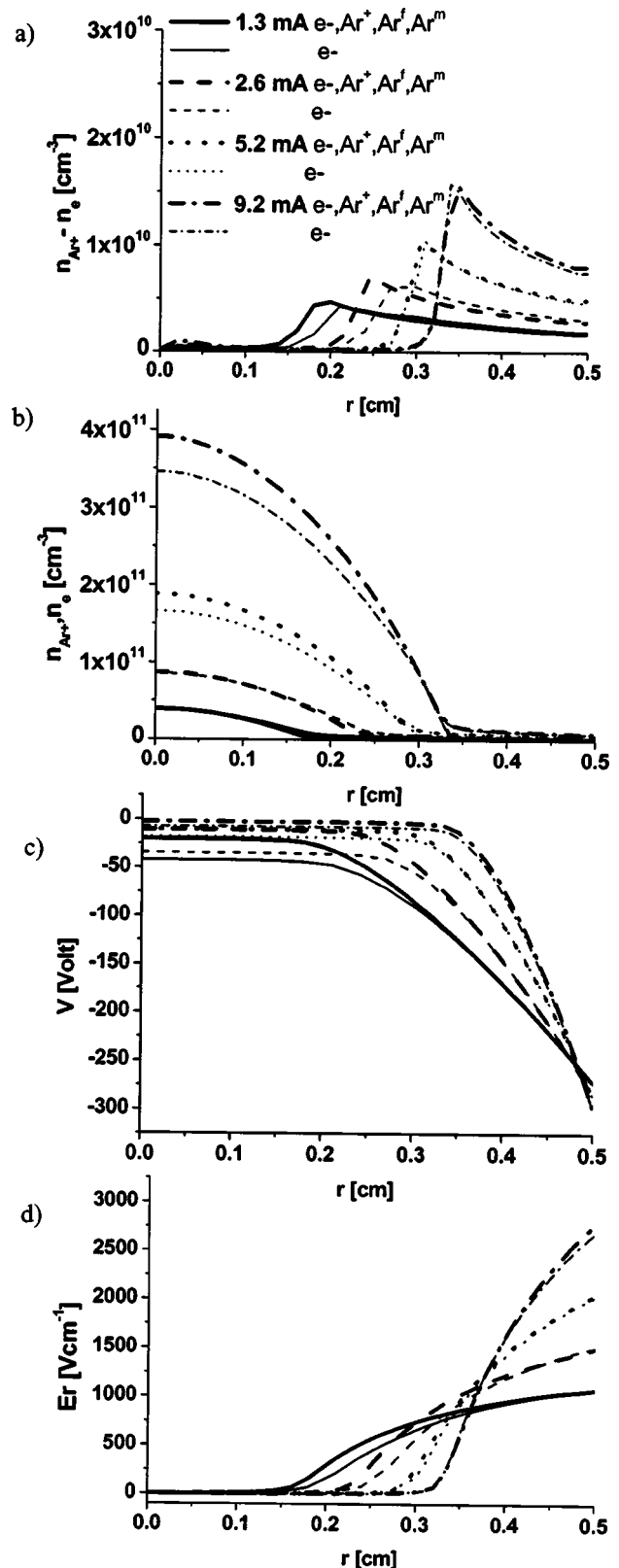


FIG. 3. Calculated radial profiles at the discharge center ( $z = 1.6$  cm) of the calculated net positive charge density (a); ion and electron densities (b); electric potential distribution (c); and electric field distribution (d) for different discharge currents at 0.3 Torr. The thick lines represent the results calculated when considering the ionization due to electron, ion, and fast atom impact collisions and metastable–metastable atom collisions, while the thin lines correspond to the model where only electron impact ionization was considered.

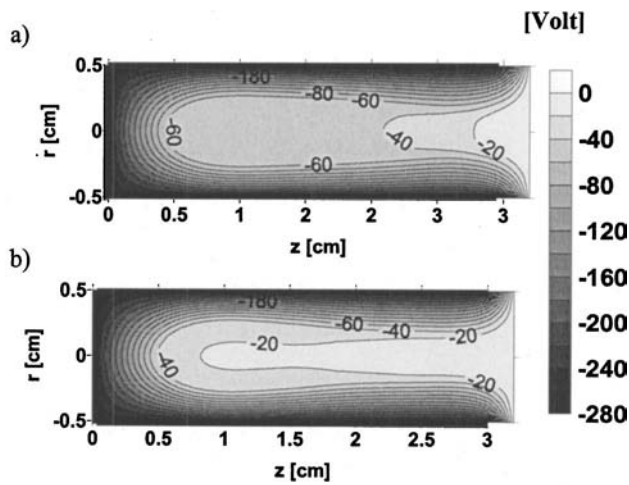


FIG. 4. Calculated two-dimensional potential distribution throughout the discharge at 1.3 mA and  $-271$  V applied voltage at a pressure of 0.3 Torr, considering the ionization due to electron impact collisions (a); and considering the ionization due to electron, ion, fast atom, and metastable-collision ionization (b).

cylinder axis, whereas  $r=0.5$  cm denotes the cathode walls. The thick lines present the results calculated when ion, fast atom, metastable, and electron ionization collisions were considered, whereas the thin lines correspond to the calculation results when only electron impact ionization was included for the same discharge conditions. Figure 3(a) shows that when the additional processes are included, especially at low current (1.3 and 2.6 mA), the net (positive) charge density increases. This will give rise to an increase in the potential drop in the CDS. Hence the plasma potential becomes less negative and consequently the radial electric field in the CDS increases, as can be observed from Figs. 3(c) and 3(d), respectively. At high currents a rise in the ion and electron density in the NG is observed [see Fig. 3(b)], as a consequence of the rise in electron impact ionization in this region. However, this rise does not influence the electric field because the net space charge does not change.

To illustrate the effect of the additional ionization mechanisms in the entire discharge, Fig. 4 shows the two-dimensional (2D) potential distributions for a discharge current of 1.3 mA and an applied voltage of  $-271$  V. Figure 4(a) presents the results for the case where only electron impact ionization was considered, whereas in Fig. 4(b) the other ionization collisions were also included. In Fig. 4(a) the equipotential curve at the NG-CDS interface corresponds to  $-60$  V, giving a potential drop in the CDS of  $-211$  V. The plasma potential at the cylinder center was equal to about  $-40$  V. In Fig. 4(b), on the other hand, the potential is equal to  $-40$  V at the CDS-NG interface, yielding a potential drop in the CDS of  $-231$  V and the plasma potential is about  $-20$  V. The CDS length does not change, hence this gives rise to an increase in the electric field in the CDS.

In Fig. 5 the 2D profiles of the mean energy of the fast  $\text{Ar}^+$  ions (a), fast Ar atoms (b), and fast electrons (c) are shown at 9.2 mA, 298 V, and 0.3 Torr. The ions and atoms reach their maximum energy at the cathode walls, whereas the electrons have their maximum energy at the end of the

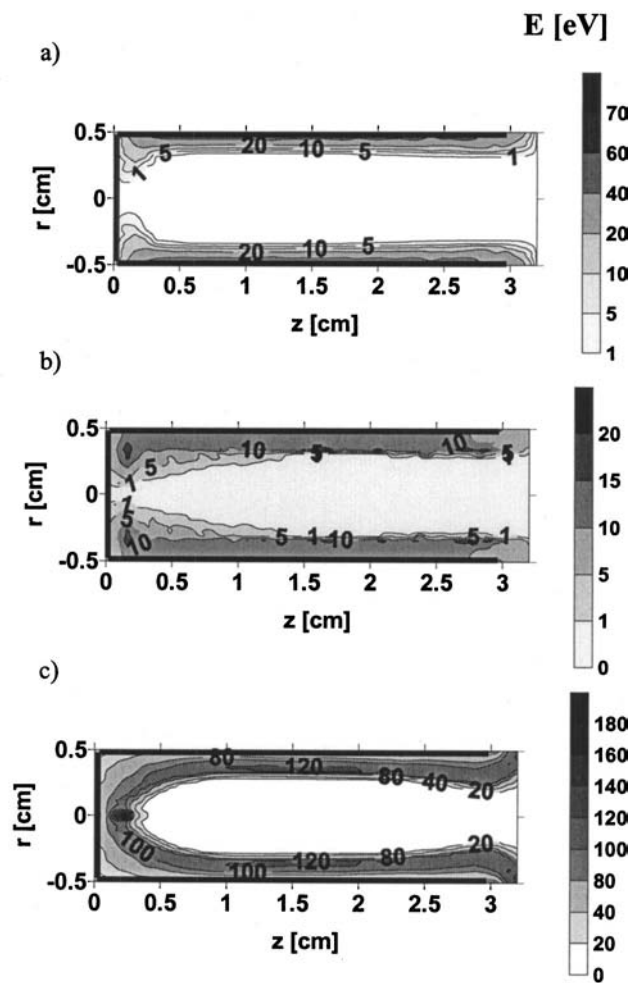


FIG. 5. Calculated two-dimensional mean energy profiles throughout the discharge at 9.2 mA of fast  $\text{Ar}^+$  ions (a); fast Ar atoms (b), and fast electrons (c) at a pressure of 0.3 Torr.

CDS because they are accelerated away from the cathode. The mean energy of the ions close to the cathode was found to be lower than the mean energy of the electrons at the CDS-NG interface because of the efficient energy transfer in the ion symmetric charge transfer collisions with the discharge gas atoms.<sup>9,13</sup> For the conditions under study, the ion mean energy at its maximum was equal to 60 eV, which corresponds to 20% of the energy associated to the potential drop in the CDS. With decreasing current, the ion mean energy drops, as is illustrated in Fig. 6. Indeed, a lower current at constant pressure arises from a lower voltage, which yields a lower energy. Moreover, the ratio of the CDS length to the mean free path of the ions for charge transfer collision ( $d/\lambda$ ) increases, so that the ion energy transfer efficiency to the neutral gas atoms increases<sup>9</sup> and consequently the ion mean energy decreases. With a rise of pressure at constant current,  $d/\lambda$  increases considerably; hence the ion mean energy decreases. This follows clearly when comparing Fig. 6(a) with Fig. 6(b) and it explains why at a pressure of 1 Torr the rate of the ion and atom impact ionization collisions was so low (see Fig. 2).

The mean energy of the fast Ar atoms is lower than the mean energy of the  $\text{Ar}^+$  ions because they are formed from

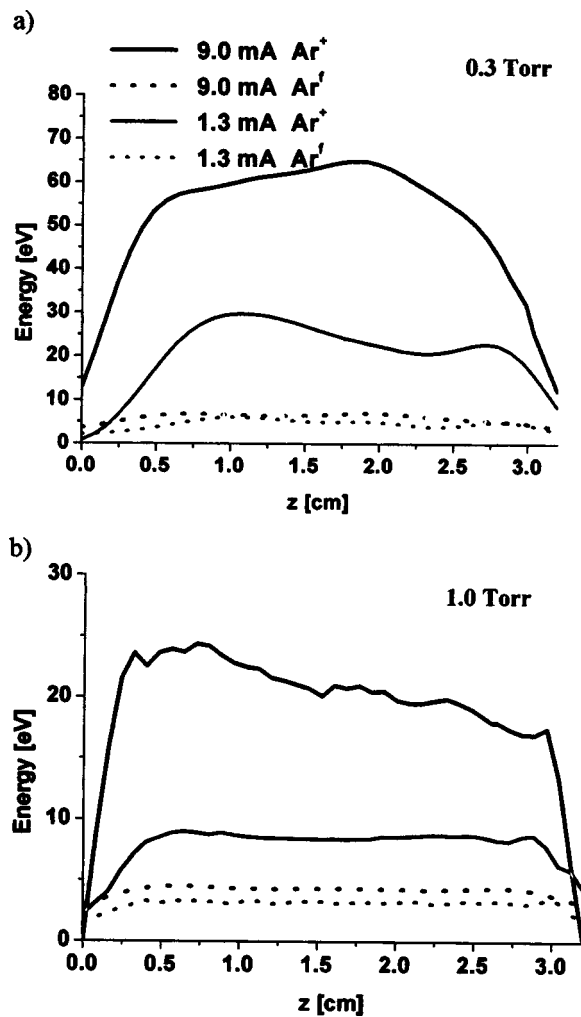


FIG. 6. Calculated  $\text{Ar}^+$  ion and fast Ar atom mean energies at the cathode wall for a current around 1 and 9 mA, and at two different pressures: 0.3 Torr (a) and 1 Torr (b). In these figures the solid lines represent the ion mean energy and the dashed lines correspond to the fast atom mean energy.

the ions as a result of elastic (including symmetric charge transfer) collisions but they are not able to gain additional energy from the electric field [see Figs. 5(b) and 6]. Close to the CDS–NG interface the fast atom mean energy increases toward the cathode wall, following the pattern of the ion energy, but further inside the CDS, their energy is more uniformly distributed than the ion energy, due to the energy broadening effect from the elastic collisions.<sup>45</sup> This is clearly illustrated in Fig. 5(b). The fraction of the maximum fast atom mean energy which respect to the energy corresponding to the CDS potential drop was found to be independent of the discharge current and changes only slightly with pressure: from 4% at 1 Torr to 5% at 0.3 Torr. In the NG no fast atoms were found.

In Fig. 5(c) we see that the mean energy of the fast electrons at the CDS–NG interface was equal to 180 eV, which corresponds to 61% of the cathode fall potential. With decreasing current this percentage decreases slightly, for example, at 1.3 mA it represents 54% of the cathode fall potential. In the NG, at 0.3 Torr, the mean electron energy was calculated to be between 10 and 20 eV, which is higher than the threshold of inelastic collisions. With rising pressure, the

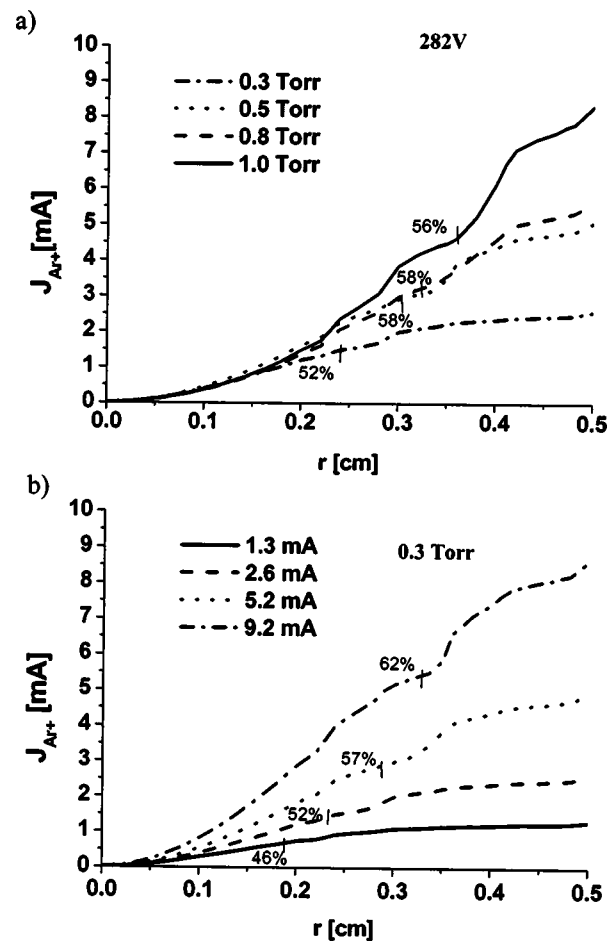


FIG. 7. Calculated radial ion current at constant applied voltage for different pressure values (a) and at constant pressure for four different currents (b). In the figures are also indicated the position corresponding to the CDS–NG interface (small vertical line) and the ratio of the ion current at the CDS–NG interface to its value at the cathode wall (expressed in percent).

electron mean energy decreases due to (i) the decrease of the applied voltage and (ii) the increase of the ratio of the CDS length to the fast electron energy relaxation length. The latter is determined by the total inelastic collision cross section because the energy exchange in the elastic collisions is negligible.<sup>46</sup> At 1 Torr the mean energy of the fast electrons in the NG was between 5 and 10 eV. Hence this is not enough to ionize the discharge gas. This explains why at 1 Torr the maximum of all inelastic collisions was found close to the CDS–NG interface, while at 0.3 Torr this maximum was located at the discharge axis.

To investigate which fraction of the total ion flux arrives from the NG at the CDS–NG interface, we have plotted in Fig. 7 the radial ion current at different pressures for a constant applied voltage (a), and at different currents for a constant pressure (b). In the figures is also indicated the position of the CDS–NG interface (small vertical lines), which was determined in our model based on the position where the ion and electron densities begin to increase and become almost equal [see Figs. 3(a) and 3(b)]. Furthermore, the ratio of the ion current at the beginning of the CDS to its value at the cathode wall, expressed in percent is also indicated. At constant voltage, this fraction was found almost independent of

the pressure [Fig. 7(a)]. At constant pressure, this value increases with rising current [Fig. 7(b)]. Indeed, at higher currents (i.e., higher voltage) the major increase in the ion current occurs in the NG, whereas at lower current, when the CDS length is larger, the major rise in current takes place inside the CDS. This is in agreement with the efficiency of electron multiplication in the CDS and in the NG, as pointed out in Ref. 28. In fact the ratio of the total ion flux coming from the NG at the CDS–NG to the total ion flux at the cathode wall is approximately equal to the ratio of the electron multiplication coefficient in the NG to the total electron multiplication coefficient in the discharge.

Concerning the importance of the different processes determining the Ar metastable density, it was found that the production was mainly due to electron impact excitation, followed by fast Ar atom impact excitation. The relative importance of the fast Ar atom impact excitation increases with rising voltage and with decreasing pressure. For example, at a current of 9 mA, Ar atom impact excitation was responsible for 14% of the production of the metastables at 1 Torr and this value rises until 31% at 0.3 Torr. The increasing role of the fast Ar atoms (and ions) in determining the metastable population at low pressures is reflected in the metastable density profile, especially at high currents. Indeed, Fig. 8 shows the 2D metastable density profiles (left set of figures) and electron impact excitation rates to the metastable level (right set of figures), for four different conditions (i.e., 1 and 0.3 Torr and for each pressure: at 1 and 9 mA). It is clear from this figure that the density profile is similar to the rate profile, for the current of 1 mA (at both pressures), suggesting that electron impact excitation is the dominant process for these conditions. On the other hand at the current of 9 mA, especially at 0.3 Torr the density profile does not overlap with the electron impact excitation rate profile, but it shows a maximum close to the cathode, where fast Ar atom and ion impact excitation occur. This result indeed indicates that fast Ar atom (and ion) impact excitation plays an increasing role at high current and low pressure.

The loss of the metastable atoms is mainly determined by quenching to the nearby resonant levels due to collision with slow electrons, as well as by diffusion to the walls and subsequent deexcitation. The metastable density was found to be in the same order of magnitude as the density of charged particles, i.e., in the order of  $10^{11} \text{ cm}^{-3}$ . Hence their role in the ionization of the plasma was found to be negligible. The absolute value of the metastable Ar density is almost independent of current [see Figs. 8(a), 8(c), and 8(e), 8(g)] and decreases slightly with decreasing pressure [see Figs. 8(a), 8(e) and 8(c), 8(g)]. The flux of metastable atoms to the cathode walls was found much lower than the ion flux for all the conditions [see Fig. 9]. At 1 Torr, the ratio of metastable atom flux to the ion flux at the cathode was 1/40 [Fig. 9(b)]. This ratio increases until 1/20 at 0.3 Torr [Fig. 9(a)], but still, it is too low to play a significant role in the emission of secondary electrons.<sup>33</sup>

In Ref. 47 a similar metastable transport model was applied to investigate the He metastable atom behavior in a HCD at 1 Torr for the same range of currents as in the present work. It was also found that the metastable density

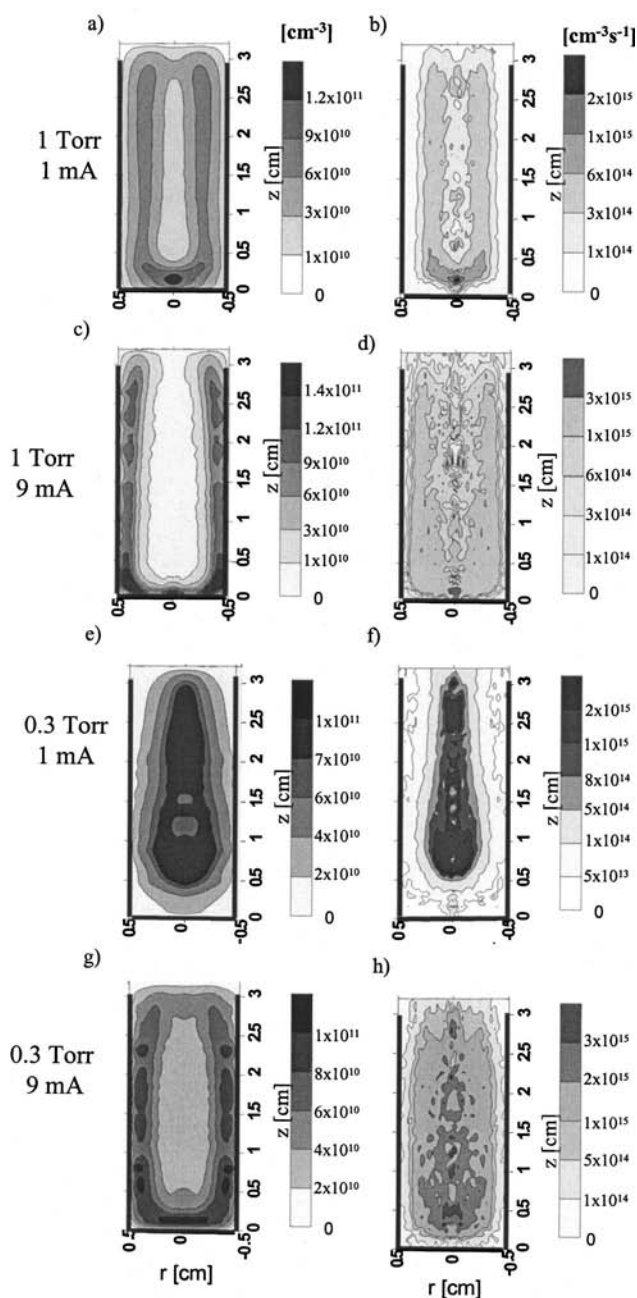


FIG. 8. Calculated two-dimensional profiles of the metastable density (left set of figures) and the electron impact excitation rate to the metastable levels (right set of figures), at two different pressures (1 and 0.3 Torr) and for each pressure at two different currents (1 and 9 mA).

increases only slightly with increasing current, but the He metastable density was one order of magnitude higher than the  $\text{He}^+$  ion and electron densities and consequently the role of metastables in secondary electron emission at the cathode and in the ionization of the discharge was rather important. The metastable–metastable ionization collisions were found to be responsible for about 20% of the total ionization in the He HCD, according to our previous model calculations.<sup>47</sup>

#### IV. CONCLUSIONS

A hybrid model, based on fluid and Monte Carlo methods, was used to describe the behavior of the electrons, ions,

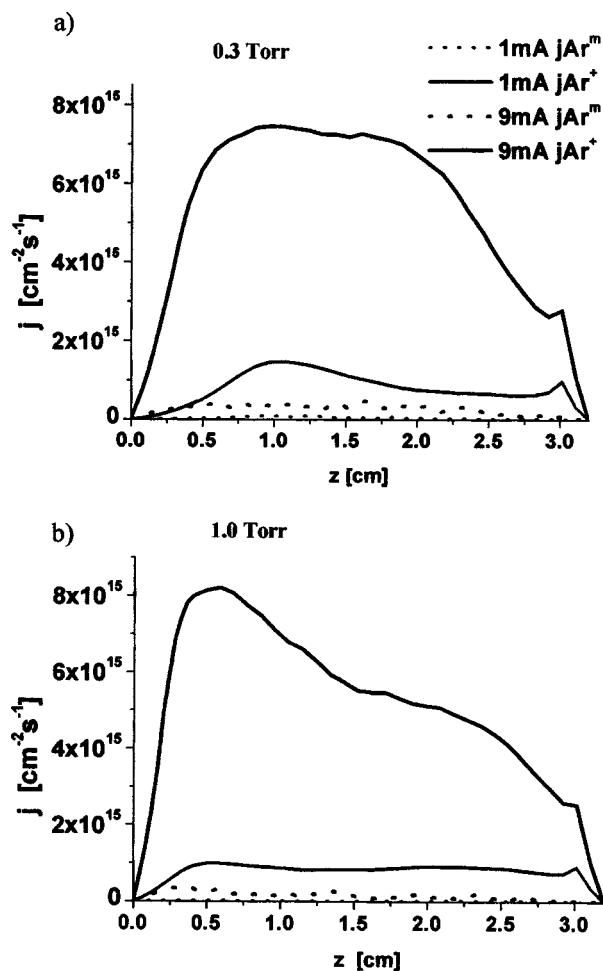


FIG. 9. Calculated ion and metastable flux densities at the cathode surface for two discharge currents at 0.3 Torr (a) and at 1.0 Torr (b). In these figures the solid lines represent the ion flux whereas the dashed lines correspond to the metastable flux.

fast atoms and metastable atoms in a cylindrical HCD with Ar as background gas. The gas pressure was varied from 0.3 to 1.0 Torr, the discharge current ranged from 1 to 10 mA and the discharge voltage was between 240 and 300 V. In a previous work,<sup>28</sup> we have analyzed in detail the fast electron behavior. We have compared the calculated current–voltage dependence and some spectrometric data of the discharge with experimental data, and good agreement was obtained. In the present work we focus on the role of the ions, fast atoms, and metastable atoms in the discharge.

We have found that integrated over the total discharge volume the ionization due to fast atoms and ions was less than 3% of the total ionization rate. The maximum in the ionization profile due to heavy particles was found very close to the cathode walls. The relative importance of these processes increases with decreasing pressure, especially at low currents, where the ionization inside the CDS is predominant. Especially for these conditions we have observed that the net positive charge density inside the CDS increases, followed by a rise in the voltage drop inside the CDS. Hence the plasma potential becomes less negative in comparison to the results obtained when only electron ionization was considered. The mean energy of fast ions, fast atoms, and fast

electrons increases with decreasing pressure and with rising current. The Ar metastable, Ar ion, and electron densities were found to be in the same order of magnitude. The main production processes determining the metastable density were found to be electron impact excitation and, with decreasing pressure and increasing current, also fast atom impact excitation. As loss sources, electron quenching and diffusion to the walls followed by deexcitation were found to be most important. The contribution of the metastable atoms to the formation of charges in the discharge is found to be negligible for the conditions under study, both as ionization source as well as in secondary electron emission from the cathode. This result is markedly different for a He HCD.<sup>47</sup>

## ACKNOWLEDGMENTS

N. Baguer and A. Bogaerts are indebted to the Flemish Fund for Scientific Research (FWO) for financial support. This research is sponsored by NATO's Scientific Affairs Division in the framework of the Science for Peace Program, by the FWO research project G.0043.01, and by the Federal Services for Scientific, Cultural and Technical Affairs of the Prime Minister's Office through IUAP V.

- <sup>1</sup>I. G. Ivanov, E. L. Latush, and M. F. Sem, *Metal Vapors Ion Lasers: Kinetic Processes and Gas Discharges* (Wiley, Chichester, 1996).
- <sup>2</sup>N. K. Vuchkov, K. A. Temelkov, and N. V. Sabotinov, *IEEE J. Quantum Electron.* **35**, 1799 (1999).
- <sup>3</sup>P. J. Slevin and W. W. Harrison, *Appl. Spectrosc. Rev.* **10**, 201 (1975).
- <sup>4</sup>S. Caroli, *Prog. Anal. At. Spectrosc.* **6**, 253 (1983).
- <sup>5</sup>D. M. Manos and D. L. Flamm, *An Introduction to Plasma Etching* (Academic, New York, 1989).
- <sup>6</sup>A. Goldamn and J. Amoroux, *Gases: Macroscopic Processes and Discharges* (Plenum, New York, 1983).
- <sup>7</sup>H. Helm, *Z. Naturforsch. A* **27A**, 1812 (1972).
- <sup>8</sup>V. I. Kolobov and L. D. Tsengin, *Plasma Sources Sci. Technol.* **4**, 551 (1995).
- <sup>9</sup>W. D. Davis and T. A. Vanderslice, *Phys. Rev.* **131**, 219 (1963).
- <sup>10</sup>I. Abril, A. Gras-Marti, and J. A. Valles-Abarca, *Phys. Rev. A* **28**, 3677 (1983).
- <sup>11</sup>I. Abril, A. Gras-Marti, and J. A. Valles-Abarca, *J. Vac. Sci. Technol. A* **4**, 1773 (1986).
- <sup>12</sup>C. W. Jurgensen and E. S. G. Shaqfeh, *J. Appl. Phys.* **64**, 6200 (1988).
- <sup>13</sup>T. J. M. Boyd and J. J. Sanderson, *Plasma Dynamics* (Nelson, London, 1969).
- <sup>14</sup>A. Tran Ngoc, E. Marode, and P. C. Johnson, *J. Phys. D* **10**, 2317 (1977).
- <sup>15</sup>A. Bogaerts, M. van Straaten, and R. Gijbels, *Spectrochim. Acta, Part B* **50**, 179 (1995).
- <sup>16</sup>Z. Wronski, *Vacuum* **42**, 635 (1991).
- <sup>17</sup>M. Surendra and D. B. Graves, *IEEE Trans. Plasma Sci.* **PS-19**, 144 (1991).
- <sup>18</sup>M. Surendra, D. B. Graves, and G. M. Jellum, *Phys. Rev. A* **41**, 1112 (1990).
- <sup>19</sup>J. P. Boeuf and L. C. Pitchford, *IEEE Trans. Plasma Sci.* **19**, 286 (1991).
- <sup>20</sup>J. P. Boeuf, *J. Appl. Phys.* **63**, 1342 (1988).
- <sup>21</sup>D. Paschier and W. J. Goedheer, *J. Appl. Phys.* **74**, 3744 (1993).
- <sup>22</sup>T. J. Sommerer and M. Kushner, *J. Appl. Phys.* **71**, 1654 (1992).
- <sup>23</sup>A. C. Dexter, T. Farrell, and M. I. Lees, *J. Phys. D* **22**, 413 (1989).
- <sup>24</sup>A. Bogaerts, R. Gijbels, and W. J. Goedheer, *J. Appl. Phys.* **78**, 2233 (1995).
- <sup>25</sup>A. Bogaerts, R. Gijbels, and W. J. Goedheer, *Anal. Chem.* **68**, 2296 (1996).
- <sup>26</sup>A. Bogaerts and R. Gijbels, *Phys. Rev. A* **52**, 3743 (1995).
- <sup>27</sup>K. Tachibana, *Phys. Rev. A* **34**, 1007 (1986).
- <sup>28</sup>N. Baguer, A. Bogaerts, and R. Gijbels, *Spectrochim. Acta, Part B* **57**, 311 (2002).
- <sup>29</sup>H. A. Hyman, *Phys. Rev. A* **20**, 855 (1979).
- <sup>30</sup>H. A. Hyman, *Phys. Rev. A* **18**, 441 (1978).
- <sup>31</sup>N. J. Mason and W. R. Newell, *J. Phys. B* **20**, 1357 (1987).

- <sup>32</sup>A. V. Phelps, J. Appl. Phys. **76**, 747 (1994).
- <sup>33</sup>A. V. Phelps, J. Phys. Chem. Ref. Data **20**, 557 (1991).
- <sup>34</sup>E. W. McDaniel and E. A. Mason, *The Mobility and Diffusion of Ions in Gases* (Wiley, New York, 1973).
- <sup>35</sup>A. V. Phelps, Phys. Rev. **99**, 1307 (1955).
- <sup>36</sup>R. Deloche, P. Monchicourt, M. Cheret, and F. Lambert, Phys. Rev. A **13**, 1140 (1976).
- <sup>37</sup>C. M. Ferreira, L. Loureiro, and A. Ricard, J. Appl. Phys. **54**, 2261 (1983).
- <sup>38</sup>M. A. Biondi, Phys. Rev. **129**, 1181 (1963).
- <sup>39</sup>D. P. Lymberopoulos and D. J. Economou, J. Appl. Phys. **73**, 3668 (1993).
- <sup>40</sup>K. Tachibana, Phys. Rev. A **34**, 1007 (1986).
- <sup>41</sup>A. Phelps and J. P. Molnar, Phys. Rev. **89**, 1202 (1953).
- <sup>42</sup>D. U. Rosenberg, *Methods for the Numerical Solutions of Partial Differential Equations* (Elsevier, New York, 1969).
- <sup>43</sup>J. B. Hasted, J. Appl. Phys. **30**, 22 (1959).
- <sup>44</sup>R. R. Arslanbekov, A. A. Kudryavtsev, and R. C. Tobin, Plasma Sources Sci. Technol. **7**, 310 (1998).
- <sup>45</sup>R. S. Mason and R. M. Allot, J. Phys. D **27**, 2372 (1994).
- <sup>46</sup>R. R. Arslanbekov, A. A. Kudryavtsev, and I. A. Movchan, Sov. Phys. Tech. Phys. **37**, 395 (1992).
- <sup>47</sup>N. Baguer, A. Bogaerts, and R. Gijbels, J. Appl. Phys. **93**, 47 (2003).